

Diffraction in hadron-hadron interactions

K. Goulios^{a*}

^aThe Rockefeller University,
1230 York Avenue, New York, NY 10021, USA
(dino@physics.rockefeller.edu)

Results on soft and hard diffraction in pp and $\bar{p}p$ collisions are reviewed with emphasis on factorization and scaling properties of differential cross sections. While conventional factorization breaks down at high energies, a scaling behavior emerges, which leads to a universal description of diffractive processes in terms of a (re)normalized rapidity gap probability distribution.

1. INTRODUCTION

The wave nature of particles leads to two classes of diffractive phenomena in hadron-hadron collisions: elastic scattering and diffraction dissociation. The former, illustrated in Fig. 1, is analogous to the classical diffraction of light.

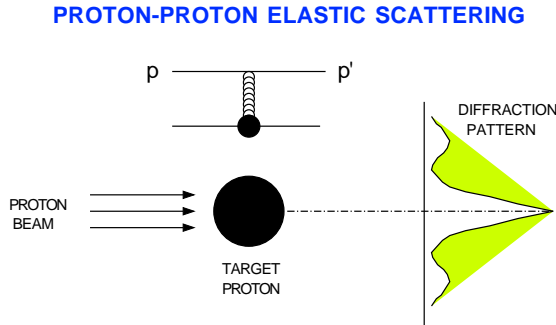


Figure 1. Illustration of diffractive pattern in small angle proton-proton scattering

For scattering by a black disc, the differential cross section is expected to have the form $d\sigma/dt \sim e^{bt}$, where $t = (p' - p)^2 \approx -p_T^2$ is the 4-momentum transfer and b the *slope parameter*. The latter is related to the disc radius, R , by $b = R^2/4$. Therefore, for a target proton of radius $\approx 1/m_\pi$, where m_π the pion mass, b is expected

*Presented at “Diffraction 2000, Cetraro, Italy, 2-7 September 2000”.

to have a value of $\frac{1}{4m_\pi^2} \approx 13 \text{ GeV}^{-2}$. This is indeed approximately what is observed, as shown in Fig. 2.

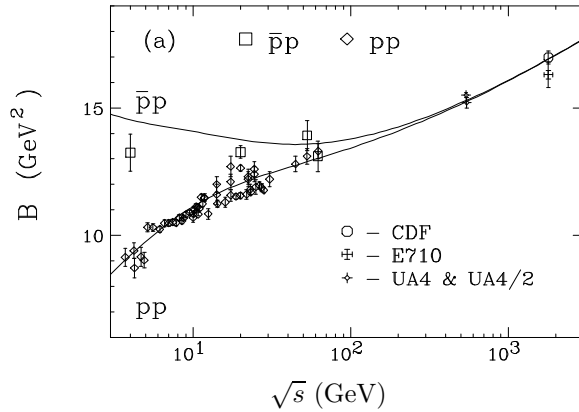


Figure 2. The slope parameter of pp and $\bar{p}p$ elastic scattering in the region of $|t| < 0.13 \text{ GeV}^2$ [1].

In contrast to elastic scattering, the phenomenon of diffraction dissociation, predicted by M.L. Good and W.D. Walker in 1960 [2], has no classical analogue. It can be thought of as the quasi-elastic scattering between two hadrons, where one of the hadrons is simultaneously excited into a higher mass state retaining its quantum numbers. This *coherent* excitation, illustrated in Fig. 3, requires not only small transverse but also small longitudinal momentum transfer. The *coherence condition* [3] is that the longitudinal momentum transfer be smaller than the in-

verse of the longitudinal proton radius, $\Delta P_L < \frac{1}{R_L} \approx m_\pi \cdot \frac{P_0}{m_p}$. In terms of the fractional longitudinal momentum loss of the quasi-elastically scattered proton, ξ , which is related to the diffractive mass M by $\xi \approx M^2/s$, the coherence condition for diffraction takes the form

$$\xi \approx \frac{M^2}{s} < \frac{m_\pi}{m_p} \approx 0.15 \quad (1)$$

The well known large increase of the $d\sigma/d\xi$ distribution in pp interactions in the region $\xi < 0.15$, which approximately exhibits the form $\frac{d\sigma}{d\xi} \propto \frac{1}{\xi}$ (see Fig. 2 of Ref. [3]), is testimony to the occurrence of a coherent phenomenon.

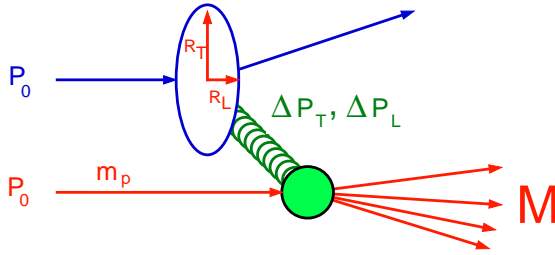


Figure 3. Illustration of diffraction dissociation.

While the wave nature of particles can explain the exponential behaviour of the forward (quasi)elastic scattering as well as the coherence condition of Eq. 1, it provides no clue for the $1/\xi$ shape of the $d\sigma/d\xi$ distribution. The ξ behaviour can be understood in terms of the nature of the exchanged “particle”, which for diffractive scattering, where no quantum numbers are exchanged, must have the quantum numbers of the vacuum. In QCD, this “particle”, which we will generically refer to here as the *Pomeron*, is a construct of (anti)quarks and gluons in a color singlet state with vacuum quantum numbers. Since such a construct does not radiate as it traverses rapidity space,² a rapidity gap (region of rapidity devoid of radiation, i.e. of particles) is associated with the exchange of a Pomeron. The width of

²We use *pseudorapidity* as an approximation to *rapidity*. Pseudorapidity is defined as $\eta \equiv \ln \frac{2p_L}{p_T}$, where p_L and p_T are the longitudinal and transverse components of the momentum of a particle with respect to the beam direction.

the rapidity gap, measured from the rapidity of the scattered (leading) proton to that of the emitted Pomeron, is given by $\Delta\eta \approx \ln \frac{1}{\xi}$. The event topology in pseudorapidity space for $p\bar{p} \rightarrow pX$ is shown in Fig. 4. Since, due to the absence of radiation, there is no resistance to the propagation of the Pomeron through rapidity space, the cross section should be independent of (or flat in) $\Delta\eta$, which through $\Delta\eta = \ln 1/\xi$ leads to $d\sigma/d\xi \propto 1/\xi$.

The Pomeron exchange picture also explains why the slope parameter of the t distribution of the leading hadron in diffraction dissociation is about one half of that of elastic scattering.

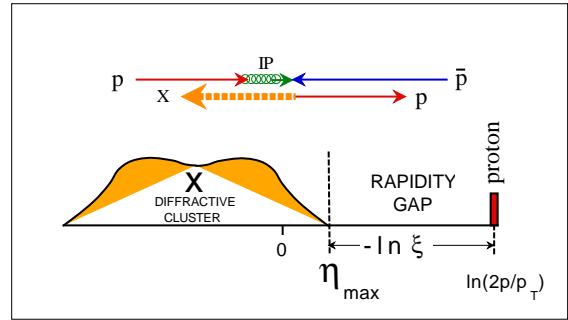


Figure 4. Event topology for $p\bar{p} \rightarrow pX$

In terms of the form factor of the $IPpp$ vertex, $F(t)$, the t dependence of elastic scattering is expected to be given by $F^4(t) \propto e^{b_{el}t}$, while for single diffraction, whose amplitude has only one $IPpp$ vertex, by $F^2(t) \propto e^{b_{sd}t}$, so that $b_{sd} = \frac{1}{2}b_{el}$.

We have seen that the main features of forward elastic scattering and of single diffraction dissociation, namely the exponential behaviour of the t distributions and the $1/\xi$ dependence, can be understood as consequences of coherent scattering resulting from the wave nature of particles or, equivalently, from an exchange with vacuum quantum numbers. However, there are subtleties in these distributions, as for example the shrinking of the forward elastic peak with increasing c.m.s. energy, whose explanation needs a theoretical framework. Such a framework has been provided by Regge theory [4]. Below, we discuss briefly some Regge theory expectations for hadronic diffraction and compare them with experimental results.

2. THE REGGE APPROACH

In the Regge theory approach [4], summarized pictorially in Fig. 5, hadronic interactions are described in terms of t -channel exchanges of Regge trajectories.

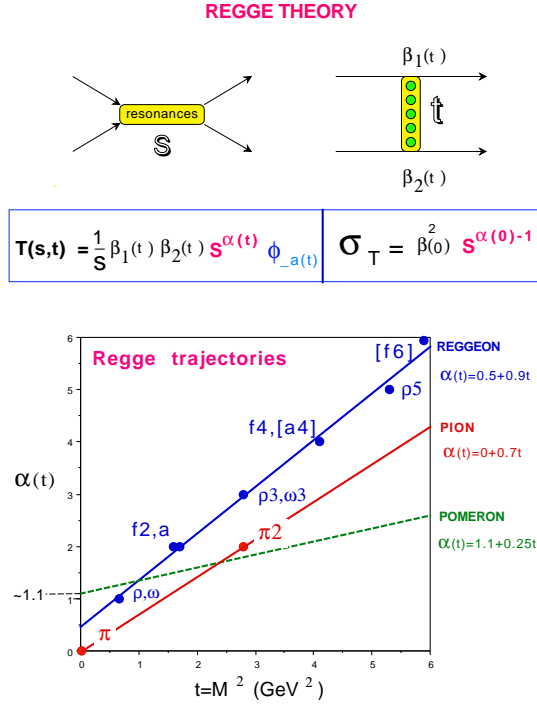


Figure 5. Summary of Regge phenomenology.

The three basic Regge trajectories are the Pion, Reggeon and Pomeron, with intercepts $\alpha(0)$ of approximately 0, 0.5 and 1.1, respectively. Because of the $s^{\alpha(t)-1}$ dependence of the amplitude $T(s, t)$ in Fig. 5, Pomeron exchange dominates at high energies. In fact, the Pomeron trajectory with $\alpha(0) \geq 1$ was introduced to account for the fact that, at high energies, hadronic cross sections were found to rise with increasing energy, rather than decrease, as would be expected from the exchange of the other Regge trajectories.

The Pomeron exchange diagrams for $\bar{p}p$ interactions are shown in Fig. 6. Through the optical theorem, the total cross section is proportional to the $t = 0$ elastic scattering amplitude.

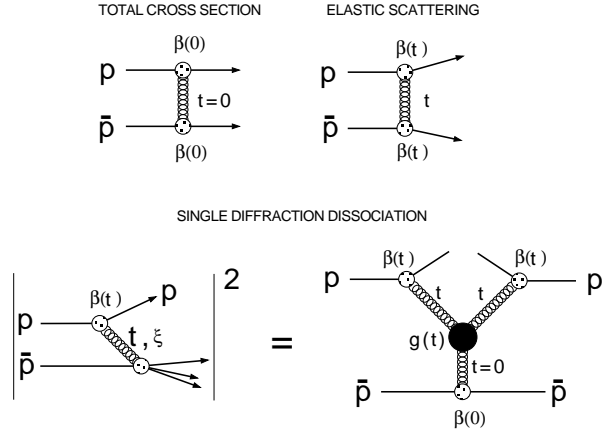


Figure 6. Diagrams for total, elastic and single diffraction dissociation cross sections.

The total, elastic and single diffractive cross sections due to Pomeron exchange are given by

$$\sigma_T(s) = \beta_{\mathbb{P}pp}^2(0) \left(\frac{s}{s_0} \right)^{\alpha_{\mathbb{P}}(0)-1} \quad (2)$$

$$\frac{d\sigma_{el}}{dt} = \frac{\beta_{\mathbb{P}pp}^4(t)}{16\pi} \left(\frac{s}{s_0} \right)^{2[\alpha_{\mathbb{P}}(t)-1]} \quad (3)$$

$$\frac{d^2\sigma_{sd}}{d\xi dt} = \underbrace{\frac{\beta_{\mathbb{P}pp}^2(t)}{16\pi} \xi^{1-2\alpha_{\mathbb{P}}(t)}}_{f_{\mathbb{P}/p}(\xi, t)} \left[\beta_{\mathbb{P}pp}(0) g(t) \left(\frac{s'}{s_0} \right)^{\alpha_{\mathbb{P}}(0)-1} \right] \quad (4)$$

where $\alpha_{\mathbb{P}}(t) = \alpha_{\mathbb{P}}(0) + \alpha' t = (1 + \epsilon) + \alpha' t$ is the Pomeron trajectory, $\beta_{\mathbb{P}pp}(t)$ the coupling of the Pomeron to the proton, $g(t)$ the $\mathbb{P}\mathbb{P}\mathbb{P}$ coupling, $s' = M^2$ the $\mathbb{P}-p$ center of mass energy squared, $\xi = 1 - x_F = s'/s = M^2/s$ the fraction of the momentum of the proton carried by the Pomeron, and s_0 an energy scale parameter traditionally set to the hadron mass scale of 1 GeV^2 .

Regge theory has been shown to provide a good description of experimental data in the Fermilab fixed target and ISR energy range ($\sqrt{s} < 60 \text{ GeV}$) [3]. However, as the energy increases, the Regge approach becomes infested with unitarity problems, which are particularly severe in the case of diffraction dissociation, as discussed in the next section.

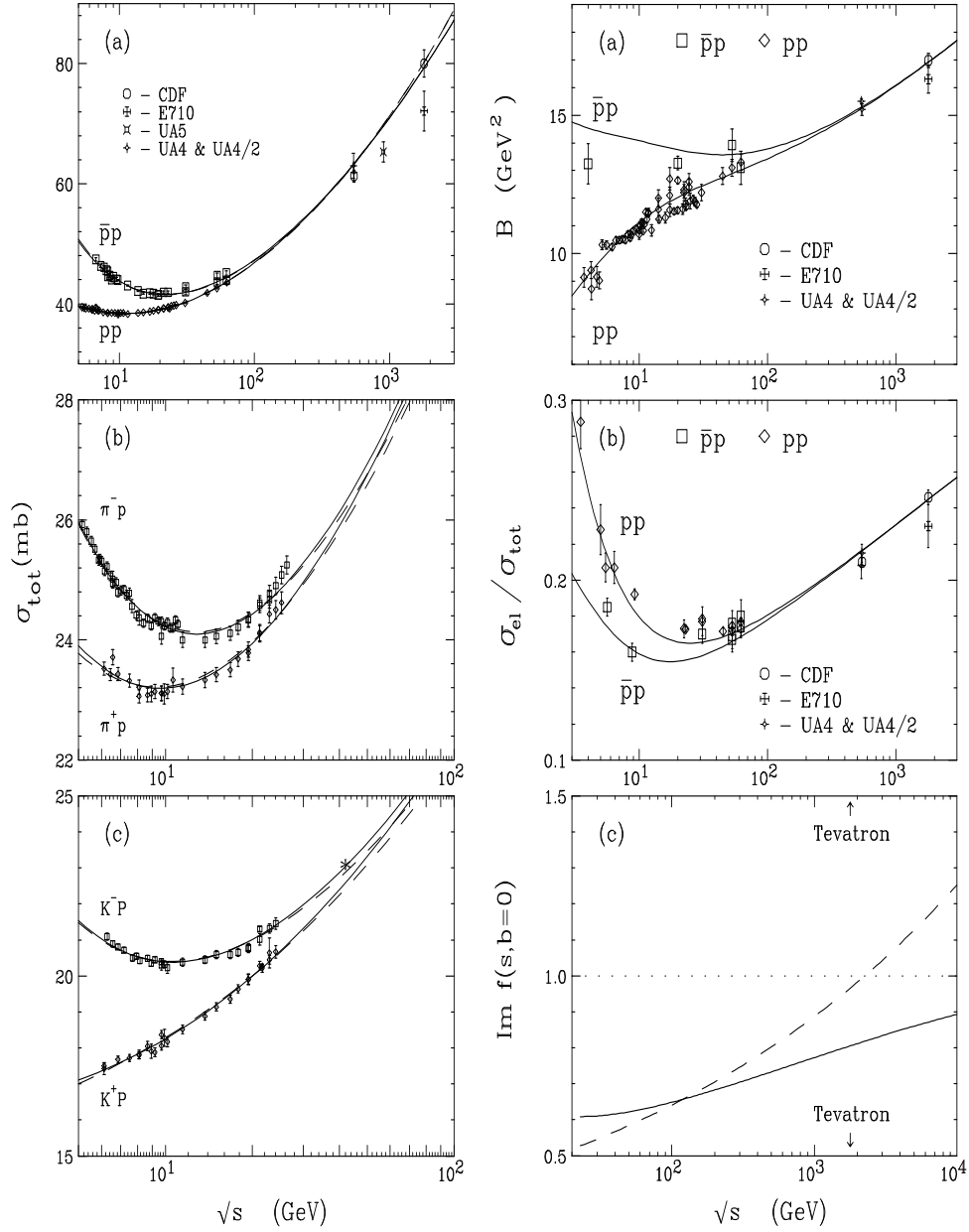


Figure 7. (*left*): $p^\pm p$, $\pi^\pm p$ and $K^\pm p$ total cross sections; (*right*): (a) slope parameter, (b) ratio of elastic to total cross section, and (c) imaginary part of elastic scattering amplitude in impact parameter space as a function of c.m.s. energy for $\bar{p}p/pp$ interactions. The dashed lines are Born level Regge fits, and the solid lines are fits after eikonilization of the elastic scattering amplitude (from Ref. [1]).

3. UNITARITY

Regge theory with a Pomeron trajectory $\alpha(0) > 1$ is plagued by unitarity problems as $s \rightarrow \infty$, namely:

(i) The power law s -dependence of the total cross section violates the Froissart bound [5]:

$$\sigma_T \propto s^\epsilon > \ln^2 s \text{ (Froissart bound)} \quad (5)$$

(ii) The elastic to total cross section ratio increases with s and violates the Pumplin bound ($\sigma_{el} < \frac{1}{2}\sigma_T$):

$$\frac{d\sigma_{el}}{dt} \propto s^{2\epsilon} e^{bt} \quad (b = b_0 + 2\alpha' \ln s) \quad (6)$$

$$\sigma_{el} \propto s^{2\epsilon} / \ln s \Rightarrow \frac{\sigma_{el}}{\sigma_T} \propto \frac{s^\epsilon}{\ln s} \quad (7)$$

(iii) The imaginary part of the forward scattering amplitude at zero impact parameter, $Im f(s, b=0)$, exceeds unity.

(iv) The ratio of single diffractive to total cross sections increases with s :

$$\frac{d\sigma_{sd}}{d\xi} \propto \frac{1}{\xi^{1+2\epsilon}} \cdot (\xi s)^\epsilon \Rightarrow \frac{d\sigma_{sd}}{dM^2} \propto \frac{s^{2\epsilon}}{(M^2)^{1+\epsilon}} \quad (8)$$

$$\frac{\sigma_{sd}}{\sigma_T} \propto s^\epsilon \quad (9)$$

In 1992, it was shown [6] that a good Regge type fit to $p^\pm p$, $\pi^\pm p$ and $K^\pm p$ cross sections, including $\bar{p}p$ cross sections at $S\bar{p}pS$ collider energies, could be obtained using two trajectories, a Pomeron and an *effective* Reggeon:

$$\sigma_T^{hp} = X s^{0.08} + Y s^{0.45} \quad (10)$$

Successful Regge type fits to single diffractive differential cross sections at Fermilab fixed target and ISR energies had already been obtained in 1983 [3] using a Pomeron trajectory with $\alpha(0) = 1$ and an effective Pion trajectory with $\alpha(0) = 0$:

$$\frac{d^2\sigma_{sd}}{d\xi dt} = \frac{A}{\xi} e^{bt} + B \xi e^{b't} \quad (11)$$

It therefore appeared that the unitarity problems inherent in Regge theory with Pomeron intercept $\alpha(0) \geq 1$ were not manifest at “present” energies. However, the situation changed in 1994 with the

CDF measurements of elastic, single diffractive and total $\bar{p}p$ cross sections at $\sqrt{s} = 540$ and 1800 GeV [7]. Although good Regge fits could still be obtained for elastic and total cross sections, two prominent unitarity problems emerged, one in elastic scattering and the other in diffraction dissociation.

In elastic scattering, the Regge prediction for the amplitude of the forward elastic scattering in impact parameter space rises with \sqrt{s} and exceeds unity at about $\sqrt{s} = 2$ TeV, violating the unitarity condition $Im f(s, b=0) \leq 1$. This problem can be brought under control by eikonalizing the elastic scattering amplitude to account for rescattering. Fig. 7 shows Born level (dashed) and eikonalized (solid) Regge fits to data [1]. Both types of fits describe the data well, but as seen in Fig. 7c the extrapolation of the Born level prediction of $Im f(s, b=0)$ to energies beyond 2 TeV violates unitarity.

Unitarity was also found to be violated by Regge fits to the $pp/\bar{p}p$ single diffractive cross sections. In their 1994 paper, the CDF Collaboration had already reported [7] that the s dependence of $d\sigma_{sd}/dM^2$ is approximately flat between $\sqrt{s} = 20$ and 540 GeV, in contrast to the Regge expectation of $s^{2\epsilon}$ behaviour (see Eq. 8). Eikonalization attempts [8] failed to provide a successful fit to the observed s -dependence (see dashed line in Fig. 8). In 1995, it was proposed [9] that the “Pomeron flux”, $f_{P/p}(\xi, t)$, represented by the first term in Eq. 4, be (re)normalized to unity when its integral over all $\xi - t$ space exceeds unity. The effect of renormalization is to practically cancel out the $s^{2\epsilon}$ dependence in $d\sigma_{sd}/dM^2$, leading to good agreement with the experimental data (see Fig. 8). The deeper physics meaning of this seemingly ad hoc renormalization proposal is discussed in the next section.

4. A SCALING LAW IN DIFFRACTION

The renormalization of the pomeron flux leads to a scaling behaviour in single diffraction, namely the s -independence of the $t = 0$ differential cross section. Figure 9 shows pp and $\bar{p}p$ single diffractive cross sections at $t = -0.05$ GeV² as a function of M^2 for different s val-

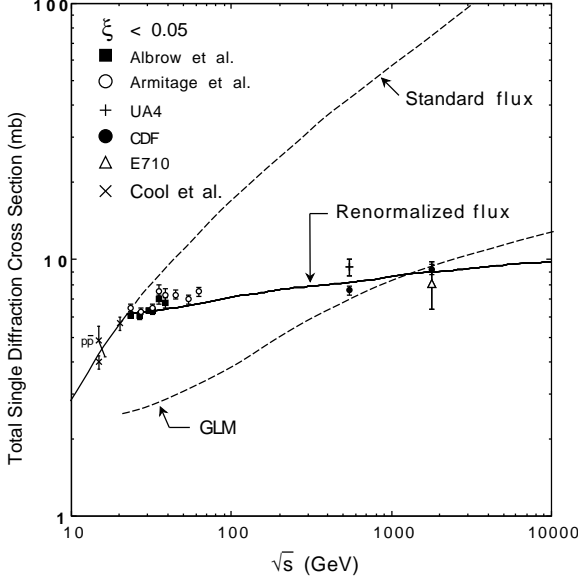


Figure 8. The total single diffraction cross section for $p(\bar{p}) + p \rightarrow p(\bar{p}) + X$ versus \sqrt{s} compared with the predictions of the renormalized pomeron flux model of Goulianos [9] (solid line) and of the model of Gotsman, Levin and Maor [8] (dashed line, labeled GLM); the latter, which includes “screening corrections”, is normalized to the average value of the two CDF measurements at $\sqrt{s} = 546$ and 1800 GeV.

ues [10]. The data have been restricted to ξ regions within which the Pomeron contribution dominates and there are no significant distortions from ξ -resolution effects. The M^2 distribution exhibits a $1/(M^2)^{1+\epsilon}$ behaviour over the entire M^2 region, which spans five orders of magnitude. The dotted lines enveloping the data represent the predictions of the renormalized Pomeron flux model using $\epsilon = 0.05$ or $\epsilon = 0.15$. The data are consistent with the same value of ϵ as that extracted from the fit of Ref. [1] to total and elastic cross sections data, namely $\epsilon = 0.104$. The Regge theory predictions for $\sqrt{s} = 540$ and 1800 GeV (dashed lines) based on extrapolation from $\sqrt{s} = 20$ GeV are significantly higher than the data.

The observed scaling behaviour acquires a physical meaning when the single diffractive cross

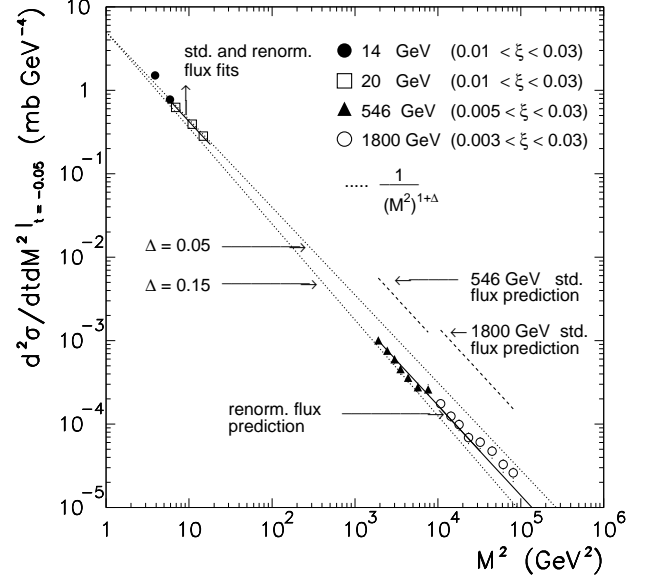


Figure 9. Cross sections $d^2\sigma_{sd}/dM^2 dt$ for $p + p(\bar{p}) \rightarrow p(\bar{p}) + X$ at $t = -0.05$ GeV² and $\sqrt{s} = 14, 20, 546$ and 1800 GeV. At $\sqrt{s} = 14$ and 20 GeV, the fits using the standard and renormalized fluxes coincide; standard (renormalized) flux predictions are shown as dashed (solid) lines.

section is written in terms of the rapidity gap, $\Delta\eta$, rather than the variable ξ , using $\Delta\eta = \ln \frac{1}{\xi}$:

$$\frac{d^2\sigma_{sd}}{dt d\Delta\eta} = \underbrace{\frac{\beta^2(t)}{16\pi} e^{2(\epsilon+\alpha't)\Delta\eta}}_{P(\Delta\eta,t)} \cdot \underbrace{\kappa \beta^2(0) \left(\frac{s'}{s_0}\right)^\epsilon}_{\kappa \sigma_T(s')} \quad (12)$$

In the naive parton model, in which the s^ϵ dependence of the total cross section can be understood in terms of the total number of the wee partons [11], the second term in the above equation represents the reduced energy ($\sqrt{s} = M$) cross section, multiplied by a factor $\kappa \equiv g(t)/\beta(0)$; the first term may then be interpreted as a rapidity gap probability [12]. Pomeron flux renormalization is equivalent to demanding that the integrated gap probability not be allowed to exceed unity. In this model, the factor κ is a color factor introduced to account for the fact that gap formation restricts the type of exchanges that lead to the total cross section to those of zero net color.

5. DOUBLE DIFFRACTION

A stringent test of the normalized gap probability model [12] is provided by soft double diffraction dissociation, which is illustrated in Fig. 10.

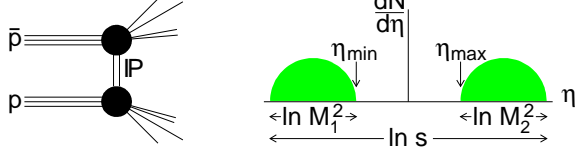


Figure 10. Schematic diagram and event topology of a double diffractive interaction, in which a Pomeron (\mathbb{P}) is exchanged in a $\bar{p}p$ collision at center-of-mass energy \sqrt{s} producing diffractive masses M_1 and M_2 separated by a rapidity gap of width $\Delta\eta = \eta_{\max} - \eta_{\min}$. The shaded areas represent regions of particle production.

From Regge theory and factorization, the cross section for double diffraction dissociation due to Pomeron exchange has the form

$$\frac{d^3\sigma_{dd}}{dt d\Delta\eta d\eta_0} = \underbrace{\frac{\kappa\beta^2(0)}{16\pi} e^{2(\epsilon+\alpha't)\Delta\eta}}_{P(\Delta\eta, \eta_0, t)} \cdot \underbrace{\kappa\beta^2(0) \left(\frac{s'}{s_0}\right)^\epsilon}_{\kappa\sigma_T(s')} \quad (13)$$

where η_0 is the center of the rapidity gap, which is “floating” between the two dissociated hadrons, and $\sqrt{s'}$ is the reduced energy given by $\sqrt{s'} = M_1 M_2 / \sqrt{s_0}$.

The only t -dependence in Eq. 13 is due to the term $e^{2\alpha't\Delta\eta}$, where the rapidity gap is given by

$$\Delta\eta = \ln \frac{ss_0}{M_1^2 M_2^2} \quad (14)$$

Since both nucleons dissociate, there is no contribution to the t -dependence from the nucleon factor factor, as is the case for single diffraction. Apart from this difference, Eqs. 13 and 12 for double and single diffraction, respectively, are strikingly similar.

The concept of Pomeron flux has no meaning in double diffraction. However, in the naive parton model view of diffraction, the first term in

CDF Preliminary

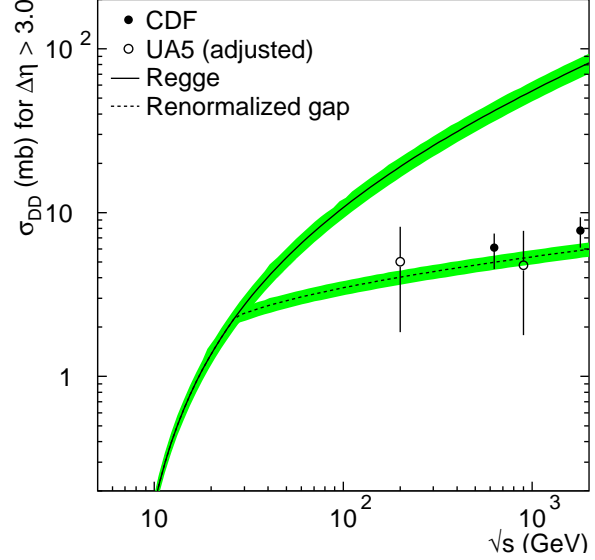


Figure 11. The total double diffractive cross section for $p(\bar{p}) + p \rightarrow X_1 + X_2$ versus \sqrt{s} compared with predictions from Regge theory based on the triple-Pomeron amplitude and factorization (solid curve) and from the renormalized gap probability model (dashed curve).

Eq. 13 can still be interpreted as a rapidity gap probability, while the second term as the reduced energy cross section multiplied by *the same* color factor κ as that measured in single diffraction. Thus, a comparison of measured double diffractive cross sections to predictions from Eq. 13 with $P(\Delta\eta, \eta_0, t)$ normalized to unity can provide an unambiguous test of the normalized gap probability model.

In Fig. 11, UA5 and preliminary CDF results [13] on double diffractive cross sections integrated over t and over all gaps for $\Delta\eta > 3$ are compared with predictions from Eq. 13 without (solid line labeled “Regge”) and with (dashed line labeled “renormalized gap”) gap renormalization. The data clearly favor the renormalized gap model.

6. THE POMERON

The introduction of the Pomeron trajectory enabled Regge theory to describe the rising total cross sections and the shrinking of the forward elastic scattering peak with increasing c.m.s. energy, as well as the shape of the single and double diffraction differential cross sections. However, a Pomeron with $\alpha(0) \geq 1$ leads to unitarity violations, which in single diffraction dissociation are already prominent at present accelerator energies. Eikonalization, which brings under control the unitarity problem associated with the high energy behaviour of elastic and total cross sections (see Fig. 7), has not been successful in dealing with single diffraction (see Fig. 8). Better results have been obtained with Gribov's Reggeon calculus approach [14], which involves multi-Pomeron exchange diagrams, but the associated calculations are cumbersome and difficult to implement in hard diffraction processes (discussed in the next section). The simplicity of Regge theory, which is its strength, is lost in the complexity of the remedies proposed to address the unitarity problem.

In contrast to the difficulties of Regge theory associated with unitarity at high energies, the data show an amazingly simple and universal s -dependence in the following two areas:

- Universality of rising cross sections:

$$\sigma_T \propto s^\epsilon$$

- Scaling behaviour in diffraction:

$$\frac{d\sigma_{sd}}{dM^2} \propto \frac{1}{(M^2)^{1+\epsilon}}$$

These two scaling laws are the key ingredients used in a new approach to diffraction [15], in which the diffractive cross section is seen as the reduced energy parton model total cross section multiplied by a color factor and a normalized rapidity gap probability.

7. HARD DIFFRACTION

Hard diffraction processes are hadronic interactions incorporating a high transverse momen-

tum partonic scattering while carrying the characteristic signature of diffraction, namely leading beam particles and/or large rapidity gaps. As in soft diffraction, such processes are believed to be mediated by Pomeron exchange. The generic QCD view of the Pomeron is a gluon/quark color-singlet state with vacuum quantum numbers. A question of great theoretical interest is whether the Pomeron has a unique particle-like partonic structure. This question can be addressed experimentally by studies of structure functions in events with a diffractive signature [16].

In hadron-hadron interactions, there are three types of hard diffraction processes accessible to experimentation with present day accelerators: single diffraction (SD), double diffraction (DD) and double pomeron exchange (DPE). The event topology of dijet events produced in these processes is shown, respectively, in Figs. 12(a), (b) and (c). All three processes can be tagged by the rapidity gap signature. Single diffraction and DPE can also be tagged by detecting the leading particle(s) on the gap side.

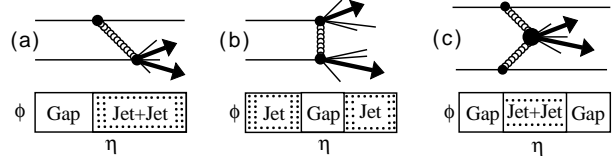


Figure 12. Dijet production diagrams and event topologies for (a) single diffraction (b) double diffraction and (c) double Pomeron exchange.

The first observation of a hard diffractive process was made by the UA8 Collaboration at the $S\bar{p}pS$ collider in a study of dijet events produced in association with a leading proton [17]. Using rapidity gap tagging, the CDF and DØ Collaborations have subsequently studied dijet production in all three processes shown in Fig. 12. In addition, CDF has studied diffractive W , b -quark and J/ψ production, as well as dijet production in SD and DPE using a “roman pot” magnetic spectrometer to detect leading antiprotons (in the DPE study the events were tagged by a leading antiproton and a rapidity gap on the proton side).

The published diffractive to non-diffractive ratios [18]–[23] obtained in the studies using rapidity gap tagging are presented in Table 1. Both the

Table 1

Diffractive to total production ratios at the Tevatron.

Hard process	\sqrt{s} (GeV)	$R = \frac{\text{DIFF}}{\text{TOTAL}}$ (%)	Comments	Exp't
SD				
$W(\rightarrow e\nu)+G$	1800	1.15 ± 0.55	$E_T^e, \cancel{E}_T > 20$ GeV	CDF [18]
Jet+Jet+G	1800	0.75 ± 0.1	$E_T^{jet} > 20$ GeV, $\eta^{jet} > 1.8$	CDF [19]
$b(\rightarrow e + X)+G$	1800	0.62 ± 0.25	$ \eta^e < 1.1, p_T^e > 9.5$ GeV	CDF [20]
DD				
Jet-G-Jet	1800	1.13 ± 0.16	$E_T^{jet} > 20$ GeV, $\eta^{jet} > 1.8$	CDF [21]
Jet-G-Jet	1800	0.54 ± 0.17	$E_T^{jet} > 12$ GeV, $\eta^{jet} > 1.6$	DØ [22]
Jet-G-Jet	630	1.85 ± 0.37	$E_T^{jet} > 12$ GeV, $\eta^{jet} > 1.6$	DØ [22]
Jet-G-Jet	630	2.7 ± 0.9	$E_T^{jet} > 8$ GeV, $\eta^{jet} > 1.8$	CDF [23]

SD and DD fractions are $\approx 1\%$ at $\sqrt{s} = 1800$ GeV and $2 - 3\%$ at $\sqrt{s} = 630$ GeV.

- The process independence of the diffractive fractions at a given energy shows that the partonic structure of the Pomeron, and in particular the gluon to quark content, is not very different from that of the proton.
- The increase of the DD fraction with decreasing energy follows the $s^{-2\epsilon}$ dependence expected from the rapidity gap (re)normalization factor. With $\epsilon \approx 0.2$, which is the value measured in diffractive DIS at HERA, the 630 to 1800 GeV ratio is predicted to be $(630/1800)^{-4\epsilon} = 2.3$, in agreement with the CDF and DØ results.

The gluon fraction of the Pomeron was measured by CDF by combining the diffractive dijet, W , and b -quark measurements. Assuming the standard Pomeron flux in the POMPYT Monte Carlo program [26], the ratios D of measured to POMPYT-predicted SD to ND fractions of W , dijet, and b -quark production rates trace different curves in the plane of D versus f_g . Figure 13 shows the $\pm 1\sigma$ curves corresponding to the results. From the oval-shaped overlap of the W , dijet and b -quark curves (shaded area), CDF obtained $f_g = 0.54^{+0.16}_{-0.14}$ and $D = 0.19 \pm 0.04$. The decrease of the value of D from HERA to the Tevatron represents a breakdown of factorization.

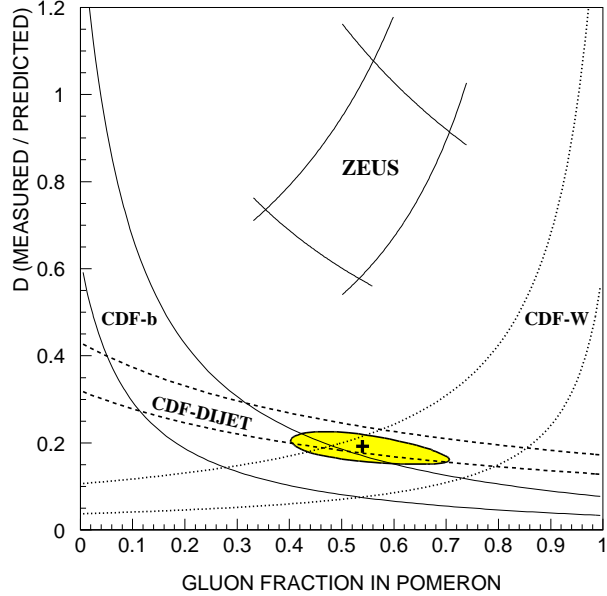


Figure 13. The ratio, D , of measured to predicted diffractive rates as a function of the gluon content of the Pomeron. The predictions are from POMPYT using the standard Pomeron flux and a hard Pomeron structure. The CDF- W curves were calculated assuming a three-flavor quark structure for the Pomeron. The black cross and shaded ellipse are the best fit and 1σ contour of a least square two-parameter fit to the three CDF results.

8. THE DIFFRACTIVE STRUCTURE FUNCTION OF THE NUCLEON

In $\bar{p}p$ collisions, the diffractive structure function (DSF) of the (anti)proton is defined in the same manner as the non-diffractive SF, except that in addition to being a function of x and Q^2 it is also a function of ξ . The DSF was measured by CDF using a sample of diffractive dijet events tagged by a leading antiproton [24]. Another event sample consisting of dijet events collected with a minimum bias trigger was used for monitoring. The procedure followed is based on measuring the ratio $R(x)$ of SD to ND cross sections as a function of the Bjorken- x of the parton in the \bar{p} participating in the hard scattering. In LO QCD, this ratio is proportional to the corresponding structure functions. The DSF is obtained by multiplying the measured $R(x)$ by the known ND structure function.

The value of x of the parton in the \bar{p} was evaluated from the jet E_T and η values, as follows:

$$x = \frac{1}{\sqrt{s}} \sum_{i=1}^n E_T^i e^{-\eta_i}$$

The sum was carried out over the two leading jets plus the next highest E_T jet, if there was one with $E_T > 5$ GeV. The structure function relevant to dijet production is a color-weighted combination of quark and gluon components:

$$F_{jj}(x) = x \left\{ g(x) + \frac{4}{9} \sum_i [(q_i(x) + \bar{q}_i(x))] \right\}$$

where $g(x)$ and $q(x)$ are gluon and quark parton densities, respectively. For comparisons with predictions based on HERA results, in which the DSF is usually presented in terms of the variable β instead of x ($\beta \equiv x/\xi$ may be interpreted as the momentum fraction of the parton in the Pomeron), the DSF obtained from the equation $F_{jj}^D(x, \xi) = R(x, \xi) \times F_{jj}^{ND}(x)$ was transformed to $F_{jj}^D(\beta, \xi)$ by a change of variables. The resulting $F_{jj}^D(\beta, \xi)$ is presented in Fig. 14 as a function of β along with expectations based on diffractive parton densities extracted by the H1 Collaboration from diffractive DIS measurements. The

CDF measured $\tilde{F}_{jj}(\beta)$ (the tilde denotes integration over the indicated ξ and t ranges) differs from the prediction based on HERA data both in shape and normalization. The normalization discrepancy is of $\mathcal{O}(0.1)$, confirming the breakdown of factorization observed in the comparison of the rapidity gap results with expectations from HERA measurements (see Fig. 13).

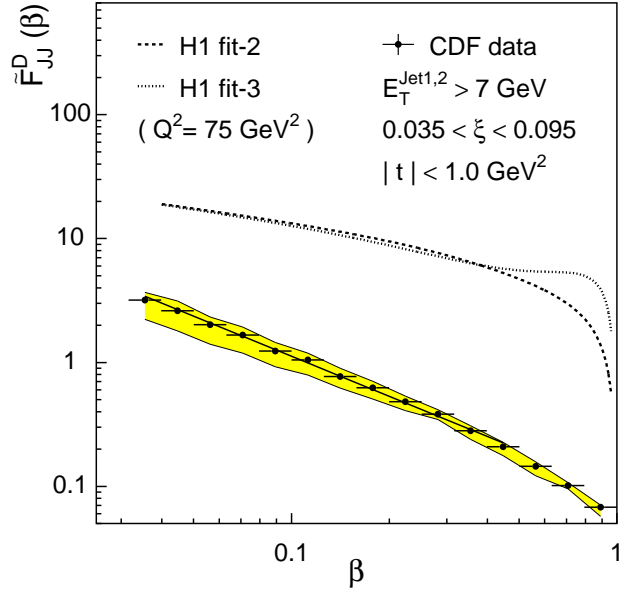


Figure 14. Data β distribution (points) compared with expectations from the parton densities of the proton extracted from diffractive deep inelastic scattering by the H1 Collaboration at HERA.

9. DOUBLE POMERON DIJETS

An interesting test of factorization has been performed by CDF by comparing the diffractive structure function measured in SD to that measured from dijet production in DPE. The DPE process is illustrated in Fig 15b. The DPE signal was extracted from the roman pot diffractive dijet event sample by requiring a rapidity gap (RG) on the proton side.

In events with a leading antiproton (LA), or equivalently with a rapidity gap on the \bar{p} side, the ratio of the DPE to SD dijet production cross sections at the same x_p for fixed ξ_p , $R_{SD}^{DPE}(x_p, \xi_p)$, is in LO QCD equal to the ratio of the SD to

ND structure functions of the proton. Therefore, diffractive factorization can be tested by comparing this ratio with the SD to ND ratio, $R_{ND}^{SD}(x_p, \xi_p)$, for SD events with no rapidity gap on the antiproton side. Since no such events were available, the comparison was made with the measured ratio $R_{ND}^{SD}(x_p, \xi_{\bar{p}})$. The result is shown in Fig. 16. The vertical dashed lines mark the DPE kinematic boundary (left) and the value of $x = \xi_p^{min}$ (right). The weighted average of the DPE/SD points in the region within the vertical dashed lines is $\tilde{R}_{SD}^{DPE} = 0.80 \pm 0.26$.

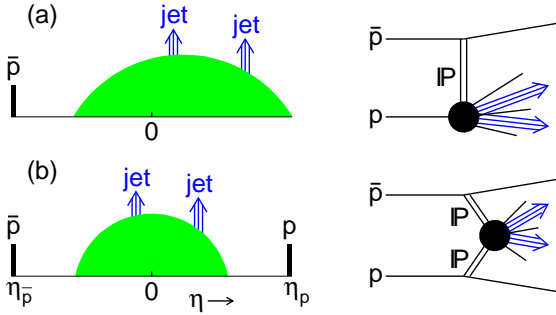


Figure 15. Illustration of event topologies in pseudorapidity, η , and associated Pomeron exchange diagrams for dijet production in (a) single diffraction and (b) double Pomeron exchange. The shaded areas on the left side represent particles not associated with the jets (underlying event).

Factorization demands that \tilde{R}_{SD}^{DPE} be the same as \tilde{R}_{ND}^{SD} at fixed x and ξ . Since the ξ_p and $\xi_{\bar{p}}$ regions, which are respectively relevant for the DPE/SD and SD/ND ratios, do not overlap, the ξ dependence of the ratios $\tilde{R}(x)$ (per unit ξ), where the tilde over the R indicates the weighted average of the points in the region of x within the vertical dashed lines in the main figure, was examined and found to be flat in ξ (see inset of Fig. 16). A straight line fit to the six \tilde{R}_{ND}^{SD} ratios extrapolated to $\xi = 0.02$ yields $\tilde{R}_{ND}^{SD} = 0.15 \pm 0.02$. The ratio of \tilde{R}_{ND}^{SD} to \tilde{R}_{SD}^{DPE} is $D \equiv \tilde{R}_{ND}^{SD} / \tilde{R}_{SD}^{DPE} = 0.19 \pm 0.07$. The deviation of D from unity represents a breakdown of factorization.

In Fig. 15, the presence of the rapidity gap on the antiproton side reduces the rapidity range over which a gap can be formed on the pro-

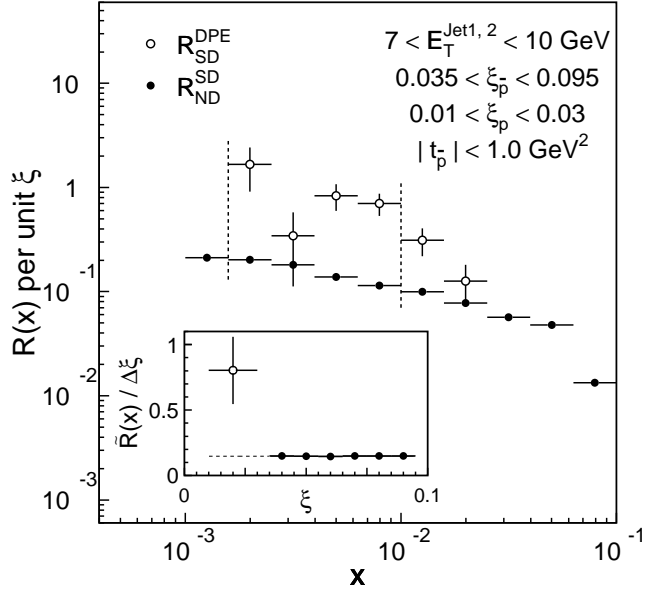


Figure 16. Ratios of DPE to SD (SD to ND) dijet event rates per unit ξ_p ($\xi_{\bar{p}}$), shown as open (filled) circles, as a function x -Bjorken of partons in the p (\bar{p}). The errors are statistical only. The SD/ND ratio has a normalization systematic uncertainty of $\pm 20\%$. The insert shows $\tilde{R}(x)$ per unit ξ versus ξ , where the tilde over the R indicates the weighted average of the $R(x)$ points in the region of x within the vertical dashed lines, which mark the DPE kinematic boundary (left) and the value of $x = \xi_p^{min}$ (right).

ton side. Thus, D decreases as the η -range available for the formation of a rapidity gap increases. This behaviour is in accordance with the (re)normalized gap probability predictions [9,12].

10. CONCLUSIONS

The central issue in hadronic diffraction is the question of universality of the rapidity gap probability. Another important issue is that of the existence of a unique, process independent diffractive structure function.

Soft single diffractive pp and $\bar{p}p$ data at low ξ and t have successfully been described [10] by the product of two terms, one proportional to the total cross section at the reduced c.m.s. energy, $\kappa\sigma_T(s')$, and the other repre-

presenting a normalized rapidity gap probability, $P(\Delta\eta, t) = P_0 e^{2(\epsilon + \alpha' t) \Delta\eta}$. Recent CDF data on double diffraction dissociation support this description [13]. Comparisons of hard diffraction results with POMPYT Monte Carlo predictions also show good agreement with the gap probability (re)normalization hypothesis. Thus, the data show a remarkable universality in rapidity gap formation extending across soft and hard processes.

The observed process independence of hard SD to ND ratios (see table 1) indicates that the partonic composition of the Pomeron is similar to that of the proton. The discrepancy in shape and normalization between the measured DSF at the Tevatron and expectations based on HERA measurements (Fig. 14) represents a breakdown of factorization. A normalization discrepancy has also been found between the DSF's measured in SD and DPE at the Tevatron. The observed discrepancy is foreseen in the RG (re)normalization model [9,12].

REFERENCES

1. A. Covolan, J. Montanha and K. Goulianos, Phys. Lett. **B 389** (1996) 176.
2. M.L. Good and W.D. Walker, Phys. Rev. **120** (1960) 1854.
3. K. Goulianos, Phys. Reports **101** (1983) 171.
4. See P.D.B. Collins, *An Introduction to Regge Theory and High Energy Physics* (Cambridge University Press, Cambridge 1977).
5. M.Froissart, Phys. Rev. **123** (1961) 1053; A.Martin, Phys. Rev. **129** (1963) 1432.
6. S. Donnachie and P.V. Landshoff, Phys. Lett. **B296** (1992) 227.
7. F. Abe *et al.*, CDF Collaboration, Phys. Rev. **D 50** (1994) 5518; **D 50** (1994) 5535; **D 50** (1994) 5550.
8. E. Gotsman, E.M. Levin and U. Maor, Phys. Rev. **D 49** (1994) R4321. **D 50**, (1994) 5535; **D 50**, (1994) 5550.
9. K. Goulianos, *Renormalization of hadronic diffraction and the structure of the pomeron*. Phys. Lett. **B 358** (1995) 379.
10. K. Goulianos and J. Montanha, Phys. Rev. **D 59** (1999) 114017.
11. E. Levin, *An Introduction to Pomerons*, Preprint DESY 98-120.
12. K. Goulianos, *Diffraction: Results and Conclusions*, in *Proceedings of LaTex International School of High Energy Physics, Rio de Janeiro, Brazil, February 16-20 1998*, edited by Andrew Brandt, H lio da Motta and Alberto Santoro; hep-ph/9806384.
13. New results presented in this talk. See also: M. Convery, FERMILAB-Conf.99/282.
14. A. Kaidalov, in these Proceedings; see also A. Kaidalov, in *Proceedings of Diffractive production in deep inelastic scattering and hadronic interactions*, VIIth Blois Workshop on Elastic and Diffractive Scattering, Ch teau de Blois, France June 20-24 1995, Editions Frontieres (P. Chiappetta, M. Haguenaue and J. Tr n Thanh V n, Eds.) pp. 107-115.
15. K. Goulianos, *Diffraction: A New Approach*, in *Proceedings of UK Phenomenology Workshop on Collider Physics, Durham, UK, September 19-24, 1999*, J. Phys. G26, 116 (2000); hep-ph/0001092.
16. G. Ingelman and P. Schlein, Phys. Lett. **B152** (1985) 256.
17. A. Brandt *et al.* (UA8 Collaboration), Phys. Lett. **B297** (1992) 417; R. Bonino *et al.* (UA8 Collaboration), Phys. Lett. **B211** (1988) 239.
18. F. Abe *et al.*, CDF Collaboration, Phys. Rev. Lett. **78** (1997) 2698.
19. F. Abe *et al.*, CDF Collaboration, Phys. Rev. Lett. **79** (1997) 2636 .
20. T. Affolder *et al.*, CDF Collaboration, Phys. Rev. Lett. **84** (2000) 232.
21. F. Abe *et al.*, CDF Collaboration, Phys. Rev. Lett. **80** (1998) 1156.
22. S. Abachi *et al.*, D  Collaboration, Phys. Lett. B **440** (1998) 189.
23. F. Abe *et al.*, CDF Collaboration, Phys. Rev. Lett. **81** (1998) 5278.
24. T. Affolder *et al.*, CDF Collaboration Phys. Rev. Lett. **84** (2000) 5043.
25. T. Affolder *et al.*, CDF Collaboration Phys. Rev. Lett. **85** (2000) 4215.
26. P. Bruni, A. Edin and G. Ingelman, <http://www3.tsl.uu.se/thep/pompyt/>